Biochimica et Biophysica Acta 1840 (2014) 1605–1613

Contents lists available at ScienceDirect

Biochimica et Biophysica Acta

journal homepage: www.elsevier.com/locate/bbagen

Review

Water channel structures analysed by electron crystallography ☆

Kazutoshi Tani, Yoshinori Fujiyoshi *

Cellular and Structural Physiology Institute, Nagoya University, Furo-cho, Chikusa, Nagoya, Japan

ARTICLE INFO

Article history:
Received 31 July 2013
Received in revised form 30 September 2013
Accepted 3 October 2013
Available online 10 October 2013

Keywords:
Water channel
Aquaporin
Electron crystallography
Cryo-electron microscopy
Cell adhesion

ABSTRACT

Background: The mechanisms underlying water transport through aquaporin (AQP) have been debated for two decades. The water permeation phenomenon of AQP seems inexplicable because the Grotthuss mechanism does not allow for simultaneous fast water permeability and inhibition of proton transfer through the hydrogen bonds of water molecules.
Scope of review: The AQP1 structure determined by electron crystallography provided the first insights into the proton exclusion mechanism despite fast water permeation. Although several studies have provided clues about the mechanism based on the AQP structure, each proposed mechanism remains incomplete. The present review is focused on AQP function and structure solved by electron crystallography in an attempt to fill the gaps between the findings in the absence and presence of lipids.
Major conclusions: Many AQP structures can be superimposed regardless of the determination method. The AQP fold is preserved even under conditions lacking lipids, but the water arrangement in the channel pore differs. The differences might be explained by dipole moments formed by the two short helices in the lipid bilayer. In addition, structure analyses of double-layered two-dimensional crystals of AQP suggest an array formation and cell adhesive function.
General significance: Electron crystallography findings not only have contributed to resolve some of the water permeation mechanisms, but have also elucidated the multiple functions of AQPs in the membrane. The roles of AQPs in the brain remain obscure, but their multiple activities might be important in the regulation of brain and other biological functions. This article is part of a Special Issue entitled Aquaporins.

1. Introduction

Water channels were postulated to exist because some biological membranes are more permeable to water than can be explained by passive diffusion through a lipid bilayer. Using a *Xenopus* oocyte expression assay, Preston et al. [1] demonstrated that a 28-kDa membrane protein that is abundant in blood cells and renal proximal tubules [2] is permeable to water. The 28-kDa membrane protein was later dubbed aquaporin-1 (AQP1), and the identified homologues from many phyla, including bacteria, plant, and animal, currently number more than 300. To date, 13 water channels, AQP0 through AQP12, have been identified in humans. The AQP family is divided into two subgroups according to the permeated molecule. AQPs transport mainly water molecules, while aquaglyceroporins transport water, glycerol, urea, and small neutral molecules. The water channels have basic roles that alleviate the osmotic stress accompanied by the movement of ions though membranes in signal transduction, energy production, and other cell activities.

Despite the fast water conductance of AQPs, they are able to filter out ions as well as protons. Although the fast water movement through such a narrow space requires the water molecules to form a continuous line of hydrogen bonds (H-bonds), protons can easily permeate through such H-bonds simply by exchanging hydrogen bonding partners, as explained by the Grotthuss mechanism. How AQPs exclude proton permeation while maintaining their fast water permeability, however, has remained unclear. We proposed a H-bond isolation mechanism to explain the proton exclusion mechanism based on the first high-resolution structure analysis of AQP1 obtained by electron crystallography [3]. Our findings, however, were not consistent with models proposed based on computer simulations using structures analysed by X-ray crystallography. Therefore, many structural and mutational studies, and molecular dynamics (MD) simulations [4–8] have been performed to elucidate these issues. The latest reported structure of yeast AQP (Aqy1) in the presence of detergent at subangstrom resolution and MD simulations provide a new model for fast water transport while preventing proton conduction (see details in Section 3) [9]. It is difficult to elucidate the fast water permeation mechanism using this structure, however, because the structure represents almost the same features of the closed Aqy1 structure with very similar crystal conditions [10]. The water channels are membrane proteins whose structures should ideally be analysed in lipid membranes, similar to their inherent conditions. Electron crystallography is a very powerful method for structure analysis of

Abbreviations: 2D, two-dimensional; ar/R, aromatic/arginine; AQP, aquaporin; AQP4M1, long isoform of aquaporin-4 starting with Met1; AQP4M23, short isoform of aquaporin-4 starting with Met23; H-bond, hydrogen bond; MD, molecular dynamics; NPA, asparagine–proline–alanine

☆ This article is part of a Special Issue entitled Aquaporins.

* Corresponding author.
E-mail address: yoshi@cespi.nagoya-u.ac.jp (Y. Fujiyoshi).

0304-4165/$ – see front matter © 2013 Elsevier B.V. All rights reserved.
http://dx.doi.org/10.1016/j.bbagen.2013.10.007

membrane proteins in membranes, as described in the following section.

2. Electron crystallography

Henderson and Unwin [11] established the power of electron crystallography by determining the first structure of the membrane protein bacteriorhodopsin and revealing that the transmembrane region forms alpha helices. Further improvements in software and the introduction of cryo-electron microscopy allowed Henderson et al. to solve the bacteriorhodopsin structure at a resolution of 3.5 Å [12]. Application of this method to other membrane proteins provided an atomic structure of the light-harvesting complex II [13]. Although many membrane protein structures have been solved by X-ray crystallography, electron crystallography remains a very powerful tool for determining membrane protein structures for several important reasons. In particular, the advantage of electron crystallography is that the structure of a membrane protein in the lipid bilayer can be resolved under almost physiological conditions. Recent membrane protein structures determined by electron crystallography, even at medium resolution (6–10 Å), have been useful toward understanding their biological functions from a structural point of view [14–16], although higher resolution analysis is preferable.

3. Atomic structure of AQP1

As mentioned in Section 1, AQP1 was not only the first characterised water channel, but it was also the first water channel protein structure determined by electron crystallography [3]. The analysed structure revealed an unusual fold with six transmembrane helices forming a right-handed bundle, which we named the AQP fold (Fig. 1). The AQP fold comprises two tandem repeat units with a pseudo two-fold symmetry, each containing three transmembrane helices and a re-entrant loop with a half pore helix (HB or HE). The helix starts from the highly conserved asparagine–proline–alanine (NPA) motif, in which the asparagine is back bonded with the NH group of the main chain by a carbonyl group, and enters the membrane from the extracellular side or cytoplasmic side in an opposite orientation. These two repeats are connected by a long extracellular loop C on the extracellular side, and are docked to each other via an interaction between helix 2 and helix 5, as well as helical interactions by mainly proline residues of the two NPA motifs of the half-pore helices at the centre of the membrane (Fig. 1). Water channel function is strongly influenced by the stability of the interaction between helices 2 and 5, each of which has a conserved glycine residue [17]. The conserved glycine with a GxxG motif in the transmembrane helix interaction is also seen in the structures of the KcsA channel and Ca^{2+}-ATPase [18].

The AQP1 structure clearly shows a tetramer as a biological unit, and each monomer has an individual channel pore with two NPA motifs (indicated by dotted circles in Fig. 1C). Based on the structure of AQP1, we proposed that an H-bond isolation mechanism is responsible for blocking proton permeation in AQPs (Fig. 2A). In this mechanism, the water molecules in the channel are forced to orient by the electrostatic field created by the dipole moment of the two short pore helices and can smoothly form H-bonds with the amide groups of the two asparagine residues of the NPA motif by exchanging hydrogen bonding partners from adjacent water molecules, which are aligned in one line in the

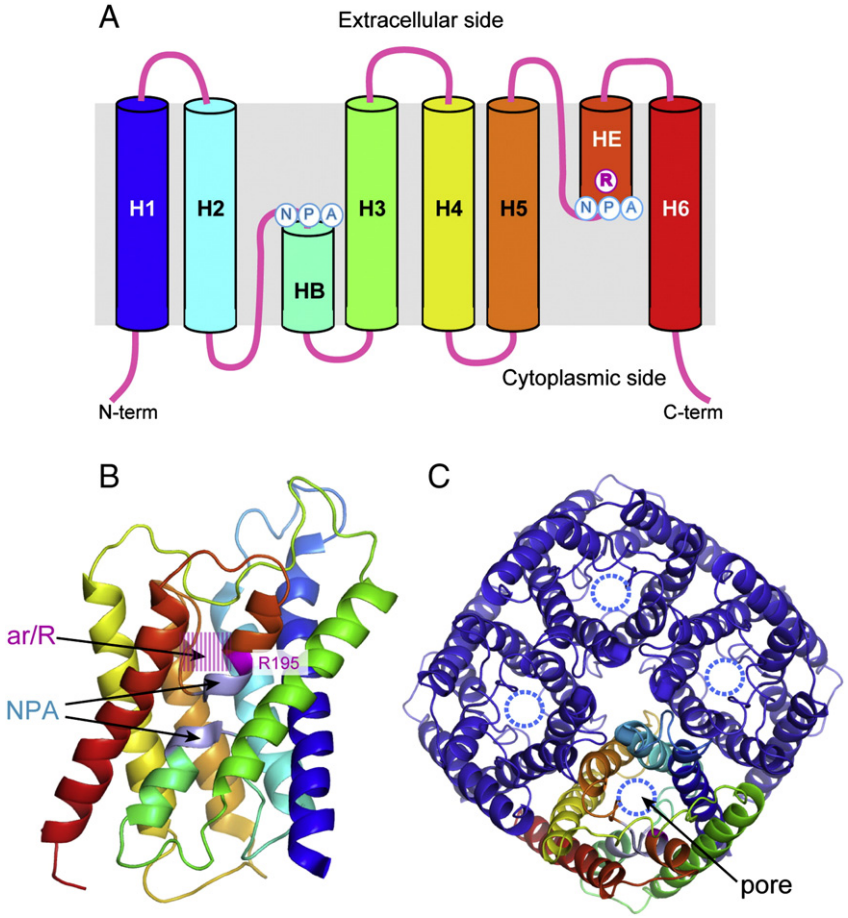

Fig. 1. Structures of AQP1 showing the typical AQP fold. (A) A secondary structure of AQP1. AQPs feature six transmembrane helices and two short pore helices, named HB and HC, which have important functions in creating the dipole moment in lipids. (B) A ribbon model of AQP1 using a rainbow colour scheme from blue (N-terminal) to red (C-terminal). The narrowest region in the AQP1 pores, previously termed ar/R [4,19], is located close to the extracellular entrance of the pore. The Arg195 and NPA motifs are shown in magenta and light blue, respectively. (C) The tetramer of AQP1 viewed from extracellular side. Each monomer has an individual pore indicated as a dotted circle.

narrow channel. This might be one important reason for the formation of the unusual characteristic AQP fold with two short pore helical arrangements, even in primitive life forms. The formation of these new H-bonds, in turn, orients the two hydrogen atoms of the water molecule in the pore constriction perpendicular to the channel axis because of the molecular orbital for water and also the arrangement of the two amide groups of the asparagine residues. This orientation might thus prevent the water molecule from forming H-bonds with the other water molecules because their arrangement perpendicular to the channel axis renders them too far away from the adjacent water molecules. Binding of the water molecules with asparagine of the NPA motif instead of adjacent water molecules reduces the energy cost for entering the narrow constriction because it affects only one H-bond relative to bulk water and allows for the transport of 3 billion or more water molecules per second and, simultaneously, the H-bond isolation blocks proton permeation. In a recent paper describing the closed yeast AQP structure at 0.88 Å resolution, MD simulations were performed with the structure, demonstrating that the water molecules do not form H-bonds with both asparagine residues of the NPAs [9]. It is an important MD result of the closed channel at the cytoplasmic side based on X-ray crystallography of the structure, and based on this study, the authors suggested that the pair-wise movement of water molecules through the channel is the predominant reason for AQPs not conducting protons.

After the H-bond isolation mechanism was proposed based on the structure determination of AQP1, other mechanisms were proposed to explain the proton exclusion by water channels [4–8]. The MD simulations by these research groups revealed the importance of the narrowest channel region other than the NPA motifs, which comprises conserved aromatic residues and a highly conserved arginine and is appropriately called the aromatic/arginine (ar/R) region [19]. The importance of the ar/R region was also suggested from the bovine AQP1 structure [20], and the proposed function of this region is as a molecular sieve based on a comparison of the diameter of ar/R between AQP1 and the glycerol-permeating channel GlpF. Recent interpretations of some MD simulations combined with mutational experiments led to the conclusion that proton exclusion is mostly due to the Arg residue at the ar/R site, and depends less on both than the Asn residues of the NPA motifs [21–23]. Another water permeation model based on the subangstrom structure of yeast AQP was recently reported by the Neutze group [9]. The authors used the high resolution structure to postulate a new model for the fast water transport while preventing proton conduction: they proposed that the four water positions at the ar/R site are too closely spaced to be simultaneously occupied [9]. Therefore, the strongly correlated movements break the connectivity of a water molecule at the ar/R site to other water molecules within the channel and prevent proton transport via the Grotthuss mechanism. Because the new structure represents almost the same features as the closed Aqy1 structure due to very similar crystal conditions [10], the structure might not represent the arrangement of water molecules in conducting channels and it is thus difficult to discuss fast water permeation with blocked proton conduction based on this model. Furthermore, the map at the ar/R site shows a continuous density, although three water molecules are assigned in this density. Therefore, the structure could not exclude hydrogen bond formation among the water molecules at this ar/R site. These structures of the water channels were fundamentally analysed by X-ray crystallography under detergent-solubilised conditions. Therefore, the analysed water positions are not the same as those in water channels analysed in a lipid bilayer by electron crystallography, as discussed in Section 5 [16,24]. Furthermore, quantitative measurement of the water permeation speed is less accurate than that of ion channels and even a simple comparison of the water permeation in two water channels, AQP1 and AQP4, remains difficult. Therefore, the mechanism of proton exclusion while allowing for fast water permeation remains unresolved.

4. Structure analyses of AQP0 and AQP4 by double-layered two-dimensional (2D) crystals

4.1. Structure of AQP0

AQP0 is abundant in eye lens fibre cells, and thus was initially named Major Intrinsic Protein [25]. In 1982, AQP0 seemed to contribute to the assembly of gap junctions due to the formation of membrane junctions [26]. Reconstitution of AQP0 into proteoliposomes induces the aggregation of vesicles [27], demonstrating the adhesive function of AQP0 in vitro. As deduced from its homology to AQP1, AQP0 is a highly specific water channel in oocytes, but its water permeation speed is much slower than that of AQP1 [28].

The first AQP0 structure from double-layered 2D crystals was resolved at 3 Å and revealed the interaction of the AQP0-mediated membrane junction [29]. The crystals were grown from a mixture of full-

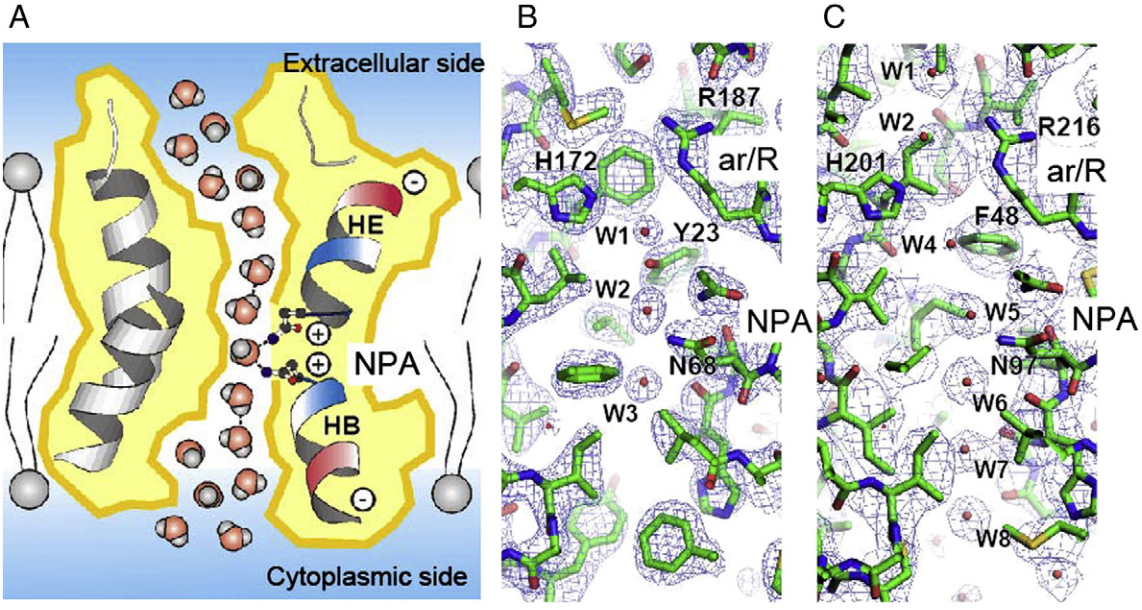

Fig. 2. Water molecules in AQPs. A: Schematic model deduced from the AQP1 structure. Adapted from [3], with permission from Nature Publishing Group. B, C: In the 2Fo–Fc map of AQP0 (B) and AQP4 (C) contoured at 1.5 and 1.2 σ (marine mesh), respectively, some water molecules in the channel (red spheres) are clearly resolved as spherical densities.

length protein and the C-terminal truncated form by proteolysis of AQP0, which increases the adhesiveness between the extracellular loops [30]. The atomic model also suggested that junctional AQP0 might be in a closed state. After improving the crystal quality as well as data collection, a 1.9-Å density map was obtained to show AQP0 in a closed conformation in which activity is interrupted by the Met76 residue extending into the pore. It also showed only three water molecules (W1–3 in Fig. 2B) in the water channel, and each was too far away from the others to form H-bonds [31]. Thus, the water molecule (W2 in Fig. 2B) can only form a H-bond with the two Asn residues of the NPA motifs. The arrangement of water molecules in the closed conformation of the AQP0 channel is consistent with the H-bond isolation mechanism. In addition, comparison with the structure of full-length AQP0 in the open conformation analysed by X-ray crystallography [32] led to the hypothesis that closure of the water channel is induced by junction formation, which, in turn, is promoted by cleavage of the C-termini [31]. MD simulations, however, suggested that junctional AQP0 can functionally maintain a water-permeable state [33,34].

4.2. Structure of AQP4

AQP4 is the predominant water channel in the brain that has a characteristic polarised distribution mainly in astrocytic endfeet, the basolateral membrane of ependymal cells, glial lamellae of the supraoptic nucleus, and other osmosensitive regions of the brain [35]. Glial cells contain characteristic orthogonal AQP4 arrays in the plasma membrane [36] that are especially prominent in glial endfeet surrounding vascular capillaries in the brain [37]. The size of the distinct crystalline patches known as orthogonal arrays in the astrocyte endfeet is regulated by the expression ratio of the two AQP4 splicing isoforms. The full-length protein starting with Met1 (AQP4M1) interferes with array formation, whereas an alternative short isoform starting with Met23 (AQP4M23) can form arrays [38,39].

The propensity of AQP4 to form ordered arrays and its predominant expression in the brain makes AQP4 an attractive target for electron crystallographic structure analysis, which was used to solve the first AQP structure and to address the puzzling questions related to the strict and fast water selective permeation functions of AQP1 [3]. AQP4 could be important for understanding complex brain mechanisms and other physiological functions, although the physiological functions of the water channel are less clear, presumably because water is the most abundant molecule in the body and also because this channel has multiple components interacting with integral elements that could at least partially underlie functional brain complexity. Therefore, the structural view of AQP4 is indispensable for facilitating comprehension of brain functions at the molecular level.

To overcome the low expression levels of AQP4 in tissues and to avoid complications due to the two AQP4 splicing variants of AQP4M1 and M23, we attempted to express rat AQP4, even though previous attempts to use expressed mammalian membrane channels for structure determination had been less successful. We successfully obtained yields of more than 3 mg of purified 6 × His-tagged AQP4M23 from 1 L of cultured Sf9 cells. Reconstitution of AQP4M23 produced large double-layered 2D arrays, which gave rise to sharp high-resolution diffraction spots and were therefore suitable for electron crystallographic structure analysis. Structure analysis was, however, complicated by variations in the lateral alignment between the two crystalline layers in the double-layered 2D crystals, making it necessary to classify the crystal types. Electron diffraction data, even with high-resolution diffraction spots, were not sensitive enough to distinguish among the crystal variants. We subsequently obtained an image of each crystal that produced a high-resolution diffraction pattern. Images providing phase information at a resolution of better than 6 Å were sufficient for distinguishing among the crystal variants. The need for a corresponding image for each diffraction pattern made the structure analysis very challenging, but our effective cryo-electron microscope system enabled us to collect all of the data required for high-resolution structure analyses [40]. Classification based on the image data identified one predominant crystal type with membrane centre-to-membrane centre spacing of 45 Å, which was selected for additional structure analysis and determined to represent approximately 70% of all of the analysed crystals. At first, 3.2 Å and later 2.8 Å resolution amplitude datasets were used to determine the AQP4 structure using the molecular replacement method [24,41].

While the structure of AQP4M23 adopts the typical AQP fold, loop C has a distinctive short 3_{10} helix that is not observed in AQP1. The narrowest region in the AQP1 pore, previously termed ar/R [4,19], is located at the same part close to the extracellular entrance of the pore. Based on the higher resolution structure of bovine AQP1 analysed by Sui et al. [20], the pore diameter of the ar/R region in AQP4 is similar to that in AQP1. At the NPA site located in the middle region of the channel, one water molecule is assumed to make H-bonds with Asn97 and Asn213 of rat AQP4 (Asn76 and Asn192 in human AQP1) by its oxygen (Figs. 2C and 3A) based on the distances between the atoms. Therefore, the water molecule at the NPA position does not seem to form an H-bond with any adjacent water molecules in either the intra- or extracellular halves of the pore. The constriction with a diameter of 3 Å at the NPA motif is just large enough to allow the passage of a water molecule whose diameter is 2.8 Å. Therefore, only one water molecule can pass through the constriction at a time and, importantly, no solutes or hydrated ions can permeate through such a narrow constriction. The AQP4 structure corroborates the H-bond isolation mechanism proposed to be responsible for blocking proton permeation while maintaining fast water permeation in AQPs [3]. The high-resolution structure also shows five lipids surrounding each AQP4 monomer and direct interactions of the extracellular surface of AQP4 with three lipids in the adjoining membrane help stabilise the membrane junction [24].

5. Single-file arrangement of water molecules in the water channel

To date, electron crystallography has resolved the structures of water molecules in two AQP channels, AQP0 and AQP4. Although the structure of AQP0 was determined at high resolution, it was analysed in a closed conformation with the Met76 residue extending into the pore [31]. Due to the closed state, AQP0 retains only three water molecules in the channel pore near the NPA motifs. In contrast, the AQP4 structure has no blocking density in the pore and the water molecules are in a single file throughout the channel. The structure of AQP4 is therefore more suitable for considering the ordinary water permeation mechanism, than that of AQP0.

The structure of AQP4 clearly resolved seven water molecules in the channel (Fig. 2C). In addition, the Fo–Fc map shows an additional spherical density at the ar/R narrowest site. Because the side-chains of AQP4 around the ar/R region are represented by a clear density and the atoms have low temperature factors in this region, we assigned the eighth water molecule (W3) to the spherical density at the ar/R site. The part of the channel with a narrow diameter is a less-favourable position for a water molecule, potentially explaining the weak density of water at this position. The two neighbouring water molecules (W2 and W4) on either side of the ar/R constriction, which form H-bonds with the unstable water molecule (W3) in the narrow region, have higher temperature factors (35 $Å^2$) compared to those of all other water molecules in the channel (2.9 $Å^2$ to 13.2 $Å^2$) (Fig. 3B).

The B-factors of the clearly observed seven water molecules in the pore are lower than 40 $Å^2$ (Fig. 3B). The quality of the density map of water molecules in the rat AQP4 structure analysed at 2.8 Å resolution by electron crystallography is better than that of water molecules in the human AQP4 structure analysed at 1.8 Å resolution by X-ray crystallography (Fig. 4). The root mean square deviation value between main chain structures analysed by electron and X-ray crystallography was 0.607 Å, and therefore the difference between the two density maps of water molecules in similar AQP4 structures analysed by two methods

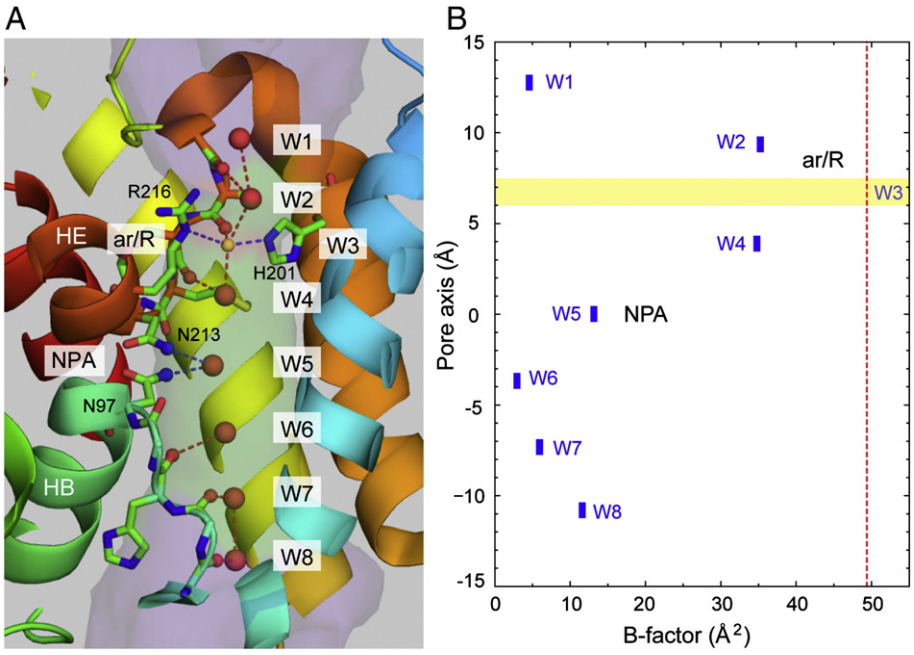

Fig. 3. Model of the water arrangement in the AQP4 channel and the temperature factors of water molecules. A: Eight water molecules from W1 to W8 in the AQP4 pore, as calculated by "HOLE", are shown as a transparent surface. The tentative position of water molecule W3, which might have a high temperature factor, is indicated by a small orange–yellow ball. Hydrogen bonds with oxygen and nitrogen are represented by red and blue dotted lines, respectively. The distances between water molecules W4 and W5 and also between W5 and W6 are clearly too long for H-bonds to form. The arrangement of these water molecules strongly supports the H-bond isolation mechanism. B: Plot of the B-factors of the water molecules in the channel. All eight water molecules in the pore are represented. Labelling of the water molecules is the same as in A. The channel region occupied by W3 is depicted as a wheat-coloured band, because the B-factor of W3 could not be determined. The red dashed line indicates the average B-factor of all the atoms in the AQP4 molecule.

counter-intuitively suggests that the lower resolution map by electron crystallography is of better quality than the map obtained by X-ray crystallography. The reason for this is not clear, but the difference in the observed map qualities for water molecules in the channel could be attributed to environmental effects. The dipole moments formed by helices, especially the two short helices HB and HE (Fig. 2A), might be influenced by the non-homogeneous environment of the lipid bilayer, as discussed by Sengupta et al. [42]. These dipole moments in the membrane layer might be much larger than those in detergent micelles and force the water molecules to orient in the water channel under the physiological conditions of the membrane interior. Although experimental proof is required to verify the effect of different environments on membrane proteins, the structure of a membrane protein determined by electron crystallography might reflect its inherent structure, because structural information can be gained in the context of a lipid bilayer, which is close to the native environment of a membrane protein.

Every exposure to the electron beam causes severe radiation damage to the specimen, and therefore each 2D crystal can only be used to collect one high-resolution image or electron diffraction pattern. Thus, to analyse the three-dimensional structure of a membrane protein, data must be collected from hundreds of 2D crystals, which is considered a disadvantage of electron crystallography. A dataset collected from multiple crystals generally causes larger error than that collected from single crystal, especially for the high-resolution reflections, because each crystal might be slightly different even though it grew under the same crystallisation conditions. Our density map obtained by electron crystallography, however, clearly but counter-intuitively resolved seven spherical densities that could unambiguously be assigned as water molecules

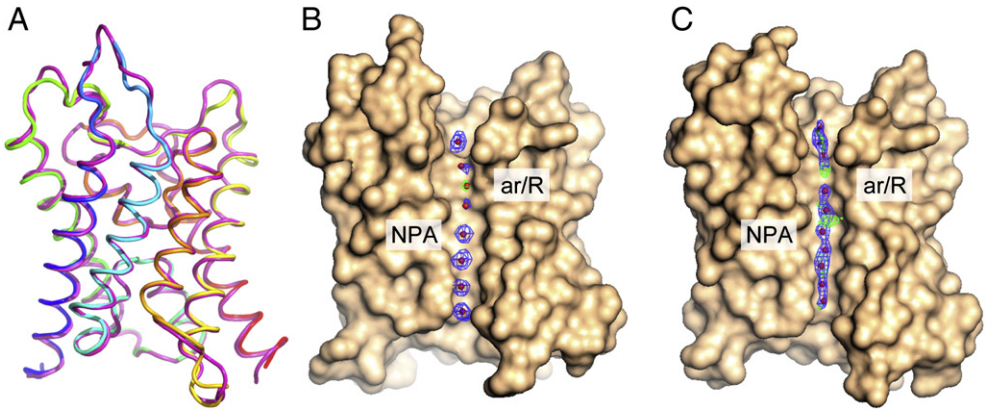

Fig. 4. Comparison of the AQP4 structure determined by electron and X-ray crystallography. A: The ribbon diagram of the structure determined by electron crystallography is shown in rainbow colours and that by X-ray crystallography is shown in magenta. B, C: The electron microscopy structure (PDB entry 2ZZ9) (B) and the X-ray structure (PDB entry 3GD8) (C) of AQP4 are represented as molecular surfaces, but H2 (cyan coloured helix in (A)) and H5 (orange coloured helix in (A)) helices of both models are removed for clarity to show the channel pathway. The water molecules in the channel are shown as red spheres. The densities of water and glycerol molecules are displayed as blue (2Fo–Fc) and green (Fo–Fc) wireframes, respectively. The water densities appear better defined in the electron microscopy map than in the X-ray map.

(Fig. 2C). The perceived weakness of electron crystallography that data must be collected from many different crystals may in fact work in our favour. We collected more than a thousand diffraction patterns, but selected only the 199 very best patterns, so that the final dataset includes only information from the very best crystals. Furthermore, while we observed diffraction spots to a resolution of 1.9 Å, we truncated the resolution of our density map to 2.8 Å to collect better data as well as to minimize the missing cone effect. Due to these procedures, the quality of the final lattice line data is exceptionally good.

Although we tried to prepare the specimens as consistently as possible during the months of data collection, there must have been variations among the specimens. As a consequence, our map represents an average of the specimen under various, slightly different conditions. As we were still able to resolve water molecules in the channel, they are presumably in defined positions. This notion is corroborated by the low temperature factors of the water molecules, ranging from 2.9 to 35.3 $Å^2$, which are significantly lower than those of the surrounding residue atoms (Fig. 3B). The same phenomenon is observed in the 1.9-Å electron crystallographic structure of AQP0 [31]. The B-factor of the water molecule associated with the amide groups of the NPA motifs is 1.7 $Å^2$, while that of the surrounding main chain atoms is in the range of 30–40 $Å^2$. The large difference in the B factors between the water and protein atoms might be due to the characteristic features of electron crystallography discussed above and/or the effect of the lipid environment enhancing the helical dipole moments.

The water positions determined in the AQP structures [20,31,32,43–45] have been superimposed on the structure of AQP4 [24] (Fig. 5). The water molecules seem to pass through the channel in a single-file arrangement, following a clearly defined route, as seen in the end-on view shown in Fig. 5B. The positions of the water molecules are not coincident with the centre lines of the channel cavity calculated by "HOLE" [46], but the position shifts close to hydrogen bonding partners. In particular, the positions of water molecules near the NPA motifs at the membrane centre deviate from the centre of the channel cavity, presumably because the water molecules make specific H-bonds with the amide groups of the asparagine residues of the NPA motifs (Fig. 5). The eight water molecules in the AQP4 channel are also in a single-file arrangement, but tend to be arranged in favourable positions, like stepping stones (Figs. 2C, 3). The inside surface of the water channels is largely hydrophobic, except for the oxygen atoms of the main chain carbonyl groups and also the nitrogen atoms of the side-chain amide groups of Asn213 and Asn97 of the NPA motifs. The eight water positions in the channel are stabilised by both the carbonyl and amide groups, which are hydrogen-bonding partners for the hydrogen and oxygen atoms, respectively, of the permeating water molecules. These partners for water molecules also form a guide rail on the hydrophobic wall of the channel fitting to the water orientation forced by dipole moments of the two half pore helices B and E (Figs. 3, 5).

The guide rail might be important molecular machinery for fast water permeation of AQP4, whose water permeation speed has been actually measured to be ~3 billion water molecules per second. The speed is similar to that of AQP1, which is one of the fastest water channels known. Based on the measured distances between successive water molecules in the channel, all water molecules appear to form H-bonds with their neighbours, except for the water molecule at the NPA site and the one below it (red dotted lines in Fig. 3A). The two hydrogen atoms of the water molecule form H-bonds with the amide groups of the asparagines (blue dotted lines in Fig. 3A), and force the water molecule to orient perpendicularly to the channel axis due to the arrangement of the amide groups and the molecular orbitals of water. The H-bonds of the water molecule (W5 in Fig. 3) at the NPA site are thus separated from the other water molecules in the channel, lending support to the H-bond isolation mechanism. Each water molecule in single-file in the channel can thus form two or three H-bonds. Water in bulk solution usually forms three or four H-bonds with neighbouring water molecules, thus they only have to sacrifice a single H-bond to enter the channel, an energy cost of about 3 kcal. The arrangement of the carbonyl and amide groups in the AQP4 channel, therefore, dramatically lowers the energy barrier for water molecules entering the narrow AQP channel and allows for very fast water permeation through the otherwise hydrophobic channel (Fig. 3). The ar/R narrowest site is important for blocking H_3O^+, but not for the separating H-bonds [21], as shown in the arrangement of water molecules in the channel (Fig. 3). Finally, if a narrow, positively-charged channel region is sufficient to

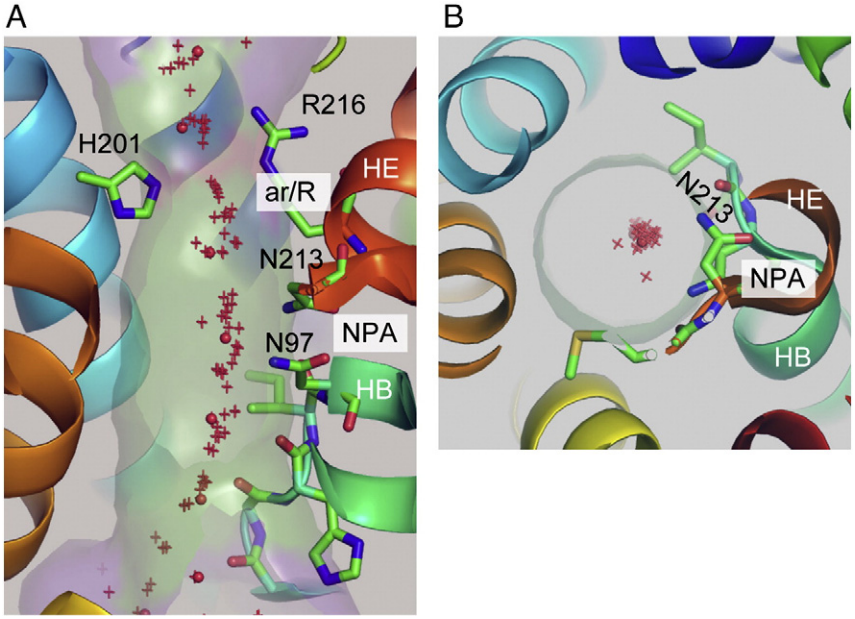

Fig. 5. AQP4 channel with the positions of all water molecules determined in AQP structures to date. The AQP4 pore as calculated by "HOLE" [46] is shown as a transparent surface. The colour indicates the pore radius from red (narrow; ar/R), green (NPA), to purple (wide). Residues interacting with water molecules in the channel are represented as stick models (carbon, oxygen, and nitrogen atoms are shown in green, red, and blue, respectively). Red crosses indicate the positions of water molecules observed in other AQP structures. Side view (A) and slice around (B) the NPA region of the AQP4 channel with water molecules observed in the structures of highly water-selective AQPs.

block proton permeation, the water channels will not have had to evolve the complex AQP fold observed in the structures of all of the water channels analysed to date.

6. Cell adhesive function of AQP0 and AQP4

AQP0 and AQP4 form double-layered 2D crystals due to interactions between the extracellular sides of the molecules (Fig. 6). These interactions are distinct from each other, and the differences might be related to their water permeation rate as well as their physiological functions. The AQP0 molecule permeates water far slower than the fast conductance type of water channel AQP1 [47]. The water conduction rate is reduced mainly by the tyrosine residue (Tyr23) interacting with water molecules in the channel pore (Fig. 2B) [31]. A tyrosine residue facing the channel has also been observed in AQP6 [48] and suggested in AQP11 [49], and MD simulations support its role in slow conductance [33,34]. In addition, all four subunits in an AQP0 tetramer can interact with the four subunits in the tetramer in the adjoining membrane as being head-to-head with respect to each other ($p422$ symmetry). Therefore, membrane junction formation can easily maintain the straight water pathway in AQP0 (Fig. 6A). Because these interactions are strong and are mediated by the three proline residues (Pro38, 109, 110), it is likely that a single pair of AQP0 molecules promotes stable membrane adhesion. These strong interactions are consistent with the absence of variations in the relative positions of the two layers in 2D crystals of AQP0. In addition, cleavage of the C-termini leads to the formation of the double-layered 2D crystals of the AQP0 [30]. Once the AQP0-mediated membrane junction forms, it is perhaps irreversibly stable.

In contrast, interactions between AQP4-adjoining molecules are formed by only two hydrophobic contacts. One is mediated by a proline at the end of membrane-spanning helix 3, which is part of a Pro–Pro motif found in AQP4 and AQP0. In AQP0, both prolines are involved in junction formation, but in AQP4, only Pro139 (corresponding to Pro110 in AQP0) contributes (Fig. 6B). A proline at the preceding position (138) is also found in AQPs 2, 5, 6, and 8, raising the possibility that these AQPs also have the potential to form membrane junctions. Val142 mediates the second interaction, which is not seen in AQP0. This residue is part of a short 3_{10} helix in the extracellular loop C (formed by residues Ser140 to Gly143), which is oriented almost parallel to the membrane surface.

The AQP4 molecule conducts water very rapidly, but membrane junction formation may increase the resistance for water conductance in AQP4 because the tetramers in the two interacting membranes are shifted with respect to each other by half a unit cell ($p42_12$ symmetry; Fig. 6B). This packing results in a tight tongue-in-groove interaction between the two membrane layers. The interaction of the tetramers in the two adjoining membranes would interfere with AQP4 water conductance due to partial blocking of the extracellular pore openings and the force generated by rapid water flow through the channels in the double-layered membranes would thus destabilise the interaction between the adjoining membranes, different from adhesive structure of AQP0 (Fig. 6A). Only a single subunit in an AQP4 tetramer can interact

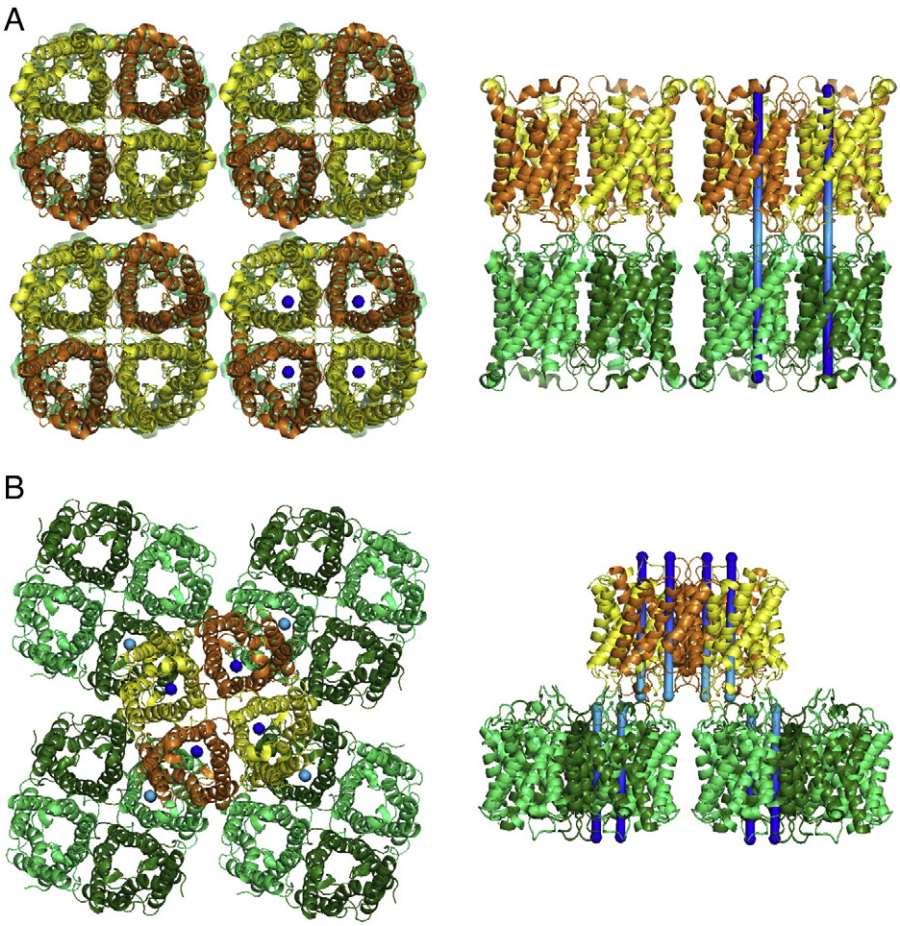

Fig. 6. Two types of double-layered interactions observed in the 2D crystals of AQP0 (A) and AQP4 (B). All adjoining molecules in AQP0 crystals can adhere even without array formation, but only one pair of molecules of AQP4 could adhere when orthogonal arrays were disrupted because the tetramer of AQP4 in the upper layer is shifted from the tetramer in the lower layer. Adjoining channels of AQP4 are shifted and water permeation is blocked when these two membrane layers are strongly adherent, in contrast to AQP0. Cylindrical objects represent water channel pathways. Blue and cyan colours indicate the cytoplasmic and extracellular side, respectively.

with a subunit in the tetramer in the adjoining membrane when the tetramer is not part of an orthogonal array. Because this interaction is mediated by only two residues and is weak, it is unlikely that a single pair of AQP4 molecules promotes stable membrane adhesion. In our crystals, each AQP4 tetramer interacts with four tetramers in the adjoining membrane, so that the formation of an orthogonal array, such as those observed in vivo, enhances the adhesive properties of AQP4. The variations in the relative positions of the two layers in our crystals, however, suggest that even crystalline AQP4 arrays promote only weak adhesion. This indicates that while the interactions between adjoining tetramers are specific (Fig. 6), the AQP4-mediated membrane junctions may be dynamic. Partially separated AQP4-containing membrane junctions have been observed in the glial laminae of the hypothalamus [50], a finding we corroborated with similar images of separated membranes within extensive membrane junction areas [41]. Because junction formation may reduce water conductance, the formation and separation of junctions may indeed be a mechanism that modulates AQP4 water conductance and/or plays a role in osmo-, thermo-, and glucose-sensing.

7. Conclusion

Electron crystallography is important for determining the structural biology of AQPs. All of the structures determined by electron crystallography can be superimposed and are very similar to corresponding structures obtained by X-ray crystallography. Based on these comparisons, we conclude that AQP folding is very stable, even in the absence of lipids. The water arrangement in the channel pore, however, is distinct in the structures determined by electron crystallography and X-ray crystallography. In addition, double-layered 2D crystal structures of AQPs suggest an array formation and cell adhesive function. Therefore, electron crystallography is necessary for revealing the complex and important functional components of AQPs that can be involved in the molecular mechanisms underlying the complex regulation of water in relation to principal biological functions. Particularly in the brain, the high water selectivity of AQPs might provide an important foundation for supporting signal transduction mechanisms regulated mainly by ion channels, but the relationship of water channels with higher order brain functions remains a mysterious and intriguing topic.

Acknowledgements

The authors thank K. Murozumi and K. Kobayashi for maintaining our electron microscopes. This research was supported by Grants-in-Aid for Young Scientists (B) (to K.T.); Grants-in-Aid for Scientific Research (S) (to Y.F.); the Japan New Energy and Industrial Technology Development Organization (NEDO) (to Y.F.); and the National Institute of Biomedical Innovation (to Y.F.).

References

[1] G.M. Preston, T.P. Carroll, W.B. Guggino, P. Agre, Appearance of water channels in Xenopus oocytes expressing red cell CHIP28 protein, Science 256 (1992) 385–387.
[2] B.M. Denker, B.L. Smith, F.P. Kuhajda, P. Agre, Identification, purification, and partial characterization of a novel Mr 28,000 integral membrane protein from erythrocytes and renal tubules, J. Biol. Chem. 263 (1988) 15634–15642.
[3] K. Murata, K. Mitsuoka, T. Hirai, T. Walz, P. Agre, J.B. Heymann, A. Engel, Y. Fujiyoshi, Structural determinants of water permeation through aquaporin-1, Nature 407 (2000) 599–605.
[4] B.L. de Groot, H. Grubmüller, Water permeation across biological membranes: mechanism and dynamics of aquaporin-1 and GlpF, Science 294 (2001) 2353–2357.
[5] E. Tajkhorshid, P. Nollert, M.Ø. Jensen, L.J.W. Miercke, J. O'Connell, R.M. Stroud, K. Schulten, Control of the selectivity of the aquaporin water channel family by global orientational tuning, Science 296 (2002) 525–530.
[6] B.L. de Groot, T. Frigato, V. Helms, H. Grubmüller, The mechanism of proton exclusion in the aquaporin-1 water channel, J. Mol. Biol. 333 (2003) 279–293.
[7] N. Chakrabarti, E. Tajkhorshid, B. Roux, R. Pomès, Molecular basis of proton blockage in aquaporins, Structure 12 (2004) 65–74.
[8] N. Chakrabarti, B. Roux, R. Pomès, Structural determinants of proton blockage in aquaporins, J. Mol. Biol. 343 (2004) 493–510.
[9] U. Kosinska-Eriksson, G. Fischer, R. Friemann, G. Enkavi, E. Tajkhorshid, R. Neutze, Subangstrom resolution X-ray structure details aquaporin–water interactions, Science 340 (2013) 1346–1349.
[10] G. Fischer, U. Kosinska-Eriksson, C. Aponte-Santamaría, M. Palmgren, C. Geijer, K. Hedfalk, S. Hohman, B.L. de Groot, R. Neutze, K. Lindkvist-Petersson, Crystal structure of a yeast aquaporin at 1.15 Å reveals a novel gating mechanism, PLoS Biol. 7 (2009) e1000130.
[11] R. Henderson, P.N. Unwin, Three-dimensional model of purple membrane obtained by electron microscopy, Nature 257 (1975) 28–32.
[12] R. Henderson, J.M. Baldwin, T.A. Ceska, F. Zemlin, E. Beckmann, K.H. Downing, Model for the structure of bacteriorhodopsin based on high-resolution electron cryo-microscopy, J. Mol. Biol. 213 (1990) 899–929.
[13] W. Kühlbrandt, D.N. Wang, Y. Fujiyoshi, Atomic model of plant light-harvesting complex by electron crystallography, Nature 367 (1994) 614–621.
[14] K. Abe, K. Tani, T. Nishizawa, Y. Fujiyoshi, Inter-subunit interaction of gastric H+, K+-ATPase prevents reverse reaction of the transport cycle, EMBO J. 28 (2009) 1637–1643.
[15] A. Oshima, K. Tani, M.M. Toloue, Y. Hiroaki, A. Smock, S. Inukai, A. Cone, B.J. Nicholson, G.E. Sosinsky, Y. Fujiyoshi, Asymmetric configurations and N-terminal rearrangements in connexin26 gap junction channels, J. Mol. Biol. 405 (2011) 724–735.
[16] Y. Fujiyoshi, Electron crystallography for structural and functional studies of membrane proteins, J. Electron Microsc. 60 (2011) S149–S159.
[17] J.B. Heymann, A. Engel, Structural clues in the sequences of the aquaporins, J. Mol. Biol. 295 (2000) 1039–1053.
[18] A.R. Curran, D.M. Engelman, Sequence motifs, polar interactions and conformational changes in helical membrane proteins, Curr. Opin. Struct. Biol. 13 (2003) 412–417.
[19] B.L. de Groot, A. Engel, H. Grubmüller, A refined structure of human aquaporin-1, FEBS Lett. 504 (2001) 206–211.
[20] H. Sui, B.-G. Han, J.K. Lee, P. Walian, B.K. Jap, Structural basis of water-specific transport through the AQP1 water channel, Nature 414 (2001) 872–878.
[21] E. Beitz, B. Wu, L.M. Holm, J.E. Schultz, T. Zeuthen, Point mutations in the aromatic/arginine region in aquaporin 1 allow passage of urea, glycerol, ammonia, and protons, Proc. Natl. Acad. Sci. U. S. A. 103 (2006) 269–274.
[22] B. Wu, C. Steinbronn, M. Alsterfjord, T. Zeuthen, E. Beitz, Concerted action of two cation filters in the aquaporin water channel, EMBO J. 28 (2009) 2188–2194.
[23] D. Wree, B. Wu, T. Zeuthen, E. Beitz, Requirement for asparagine in the aquaporin NPA sequence signature motifs for cation exclusion, FEBS J. 278 (2011) 740–748.
[24] K. Tani, T. Mitsuma, Y. Hiroaki, A. Kamegawa, K. Nishikawa, Y. Tanimura, Y. Fujiyoshi, Mechanism of aquaporin-4's fast and highly selective water conduction and proton exclusion, J. Mol. Biol. 389 (2009) 694–706.
[25] M.B. Gorin, S.B. Yancey, J. Cline, J.P. Revel, J. Horwitz, The major intrinsic protein (MIP) of the bovine lens fiber membrane: characterization and structure based on cDNA cloning, Cell 39 (1984) 49–59.
[26] D. Bok, J. Dockstader, J. Horwitz, Immunocytochemical localization of the lens main intrinsic polypeptide (MIP26) in communicating junctions, J. Cell Biol. 92 (1982) 213–220.
[27] I. Dunia, S. Manenti, A. Rousselet, E.L. Benedetti, Electron microscopic observations of reconstituted proteoliposomes with the purified major intrinsic membrane protein of eye lens fibers, J. Cell Biol. 105 (1987) 1679–1689.
[28] S.M. Mulders, G.M. Preston, P.M. Deen, W.B. Guggino, C.H. van Os, P. Agre, Water channel properties of major intrinsic protein of lens, J. Biol. Chem. 270 (1995) 9010–9016.
[29] T. Gonen, P. Sliz, J. Kistler, Y. Cheng, T. Walz, Aquaporin-0 membrane junctions reveal the structure of a closed water pore, Nature 429 (2004) 193–197.
[30] T. Gonen, Y. Cheng, J. Kistler, T. Walz, Aquaporin-0 membrane junctions form upon proteolytic cleavage, J. Mol. Biol. 342 (2004) 1337–1345.
[31] T. Gonen, Y. Cheng, P. Sliz, Y. Hiroaki, Y. Fujiyoshi, S.C. Harrison, T. Walz, Lipid–protein interactions in double-layered two-dimensional AQP0 crystals, Nature 438 (2005) 633–638.
[32] W.E.C. Harries, D. Akhavan, L.J.W. Miercke, S. Khademi, R.M. Stroud, The channel architecture of aquaporin 0 at a 2.2-Å resolution, Proc. Natl. Acad. Sci. U. S. A. 101 (2004) 14045–14050.
[33] B.G. Han, A.B. Guliaev, P.J. Walian, B.K. Jap, Water transport in AQP0 aquaporin: molecular dynamics studies, J. Mol. Biol. 360 (2006) 285–296.
[34] M.Ø. Jensen, R.O. Dror, H. Xu, D.W. Borhani, I.T. Arkin, M.P. Eastwood, D.E. Shaw, Dynamic control of slow water transport by aquaporin 0: implications for hydration and junction stability in the eye lens, Proc. Natl. Acad. Sci. U. S. A. 105 (2008) 14430–14435.
[35] M. Moghaddam, O.P. Ottersen, The molecular basis of water transport in the brain, Nat. Rev. Neurosci. 4 (2003) 991–1001.
[36] J.E. Rash, T. Yasumura, C.S. Hudson, P. Agre, S. Nielsen, Direct immunogold labeling of aquaporin-4 in square arrays of astrocyte and ependymocyte plasma membranes in rat brain and spinal cord, Proc. Natl. Acad. Sci. U. S. A. 95 (1998) 11981–11986.
[37] D.M. Landis, T.S. Reese, Membrane structure in mammalian astrocytes: a review of freeze-fracture studies on adult, developing, reactive and cultured astrocytes, J. Exp. Biol. 95 (1981) 35–48.
[38] C.S. Furman, D.A. Gorelick-Feldman, D.G. Davidson, T. Yasumura, D.J. Neely, P. Agre, J.E. Rash, Aquaporin-4 square array assembly: opposing actions of M1 and M23 isoforms, Proc. Natl. Acad. Sci. U. S. A. 100 (2003) 13609–13614.
[39] C. Silberstein, R. Bouley, Y. Huang, P. Fang, N. Pastor-Soler, D. Brown, A.N. Van Hoek, Membrane organization and function of M1 and M23 isoforms of aquaporin-4 in epithelial cells, Am. J. Physiol. Renal Physiol. 287 (2004) F501–F511.
[40] Y. Fujiyoshi, The structural study of membrane proteins by electron crystallography, Adv. Biophys. 35 (1998) 25–80.
[41] Y. Hiroaki, K. Tani, A. Kamegawa, N. Gyobu, K. Nishikawa, H. Suzuki, T. Walz, S. Sasaki, K. Mitsuoka, K. Kimura, A. Mizoguchi, Y. Fujiyoshi, Implications of the aquaporin-4 structure on array formation and cell adhesion, J. Mol. Biol. 355 (2006) 628–639.

[42] D. Sengupta, R.N. Behera, J.C. Smith, G.M. Ullmann, The α helix dipole: screened out? Structure 13 (2005) 849–855.
[43] D.F. Savage, P.F. Egea, Y. Robles-Colmenares, J.D. O'Connell, R.M. Stroud, Architecture and selectivity in aquaporins: 2.5 Å X-ray structure of aquaporin Z, PLoS Biol. 1 (2003) 334–340.
[44] S. Törnroth-Horsefield, Y. Wang, K. Hedfalk, U. Johanson, M. Karlsson, E. Tajkhorshid, R.M. Stroud, Structural mechanism of plant aquaporin gating, Nature 439 (2006) 688–694.
[45] R. Horsefield, K. Norden, M. Fellert, A. Backmark, S. Törnroth-Horsefield, A.C. Terwisscha van Scheltinga, J. Kcassman, P. Kjellbom, U. Johanson, R. Neutze, High-resolution x-ray structure of human aquaporin 5, Proc. Natl. Acad. Sci. U. S. A. 105 (2008) 13327–13332.
[46] O.S. Smart, J.G. Neduvelil, X. Wang, B.A. Wallace, M.S. Sansom, HOLE: a program for the analysis of the pore dimensions of ion channel structural models, J. Mol. Graph. 14 (1996) 354–360.
[47] G. Chandy, G.A. Zampighi, M. Kreman, J.E. Hall, Comparison of the water transporting properties of MIP and AQP1, J. Membr. Biol. 159 (1977) 29–39.
[48] M. Yasui, A. Hazama, T.H. Kwon, S. Nielsen, W.B. Guggino, P. Agre, Rapid gating and anion permeability of an intracellular aquaporin, Nature 402 (1999) 184–187.
[49] K. Yakata, K. Tani, Y. Fujiyoshi, Water permeability and characterization of aquaporin-11, J. Struct. Biol. 174 (2011) 315–320.
[50] S. Nielsen, E.A. Nagelhus, M. Amiry-Moghaddam, C. Bourque, P. Agre, O.P. Ottersen, Specialized membrane domains for water transport in glial cells: high-resolution immunogold cytochemistry of aquaporin-4 in rat brain, J. Neurosci. 17 (1997) 171–180.